Draft version February 2, 2008
Preprint typeset using LaTeX style emulateapj v. 14/09/00

arXiv:astro-ph/0209108v1 5 Sep 2002

KINEMATICS OF PLANETARY NEBULAE IN M51'S TIDAL DEBRIS

Patrick R. Durrell
pdurrell@astro.psu.edu
Department of Astronomy and Astrophysics, Penn State University, 525 Davey Lab, University Park, PA 16802
J. Christopher Mihos[1], John J. Feldmeier
hos@burro.astr.cwru.edu, johnf@eor.astr.cwru.edu
Department of Astronomy, Case Western Reserve University, 10900 Euclid Ave, Cleveland, OH 44106
George H. Jacoby
jacoby@wiyn.org
WIYN Observatory[2], P.O. Box 26732, Tucson AZ 85726
and
Robin Ciardullo
rbc@astro.psu.edu
Department of Astronomy and Astrophysics, Penn State University, 525 Davey Lab, University Park, PA 16802

accepted for publication in the Astrophysical Journal

ABSTRACT

We report the results of a radial velocity survey of planetary nebulae (PNe) located in the tidal features of the well-known interacting system NGC 5194/95 (M51). We find clear kinematic evidence that M51's northwestern tidal debris consists of two discrete structures which overlap in projection – NGC 5195's own tidal tail, and diffuse material stripped from NGC 5194. We compare these kinematic data to a new numerical simulation of the M51 system, and show that the data are consistent with the classic "single passage" model for the encounter, with a parabolic satellite trajectory and a 2:1 mass ratio. We also comment on the spectra of two unusual objects: a high-velocity PN which may be associated with NGC 5194's halo, and a possible interloping high-redshift galaxy.

Subject headings: galaxies: individual (M51) — galaxies: interactions — galaxies: kinematics and dynamics — planetary nebulae: general

1. INTRODUCTION

The "Whirlpool Galaxy," M51 (NGC 5194, 5195)[3] is probably the most famous of all interacting galaxy systems. As a nearby system ($d = 8.4 \pm 0.6$ Mpc; Feldmeier, Ciardullo, & Jacoby 1997, hereafter FCJ) with grand-design spiral morphology (Rosse 1845; see Rosse 1880), distorted outer isophotes (Zwicky 1959; Burkhead 1978), and an apparent bridge-like feature between the primary, NGC 5194, and the secondary, NGC 5195, M51 has been extensively studied as an example of tidally induced spiral structure (e.g., Tully 1974; Scoville & Young 1983; Rots et al. 1990; Zaritsky, Rix, & Rieke 1993). In fact, the wealth and detail of the observational data has made M51 a favorite target for dynamical modeling, starting with the seminal work of Toomre & Toomre (1972). In the Toomre & Toomre (1972) study, many of the tidal features of the M51 system were explained by a parabolic encounter of two galaxies with mass ratio of 3:1 viewed shortly after the initial collision. Since then, in response to the ever-increasing amount of observational data on the system, a number of alternate scenarios have been proposed (Toomre 1978; Howard & Byrd 1990; Hernquist 1990; Barnes 1998; Salo & Laurikainen 2000).

Despite M51's long history of dynamical modeling, significant uncertainties in the basic description of the system remain. While the original Toomre & Toomre (1972) study proposed a very recent ($\sim$ 100 Myr) collision, the discovery of M51's long H I tidal tail (Rots et al. 1990) shifted the preferred solution to somewhat later times (several hundred Myr past the initial collision) in order to give the tail more time to develop (Hernquist 1990). More recently, Salo & Laurikainen (2000) have suggested that a multiple passage model might be more appropriate for the system. Such a scenario appears to do a better job of explaining NGC 5194's H I velocity field, although the predicted structure for the H I tidal tail is more complex than is observed.

Furthermore, the simulations of Salo & Laurikainen (2000) used rigid halo models, which do not self-consistently follow the orbital evolution of the system. Because the multiple passage model relies on orbital decay to provide the proper second passage, the lack of a self-consistent solution remains a concern for these models. As a result, these models have not followed the full dynamical response of the system (Salo & Laurikainen 2000). Consequently, no single scenario satisfactorily explains all of the system's observational data (see the discussion in Barnes 1998).

[1] Research Corporation Cottrell Scholar and NSF CAREER Fellow

[2] The WIYN Observatory is a joint facility of the University of Wisconsin-Madison, Indiana University, Yale University, and the National Optical Astronomy Observatory.

[3] Throughout this paper, we use the designation M51 when considering both galaxies as a complete system; when referencing the system's individual components, we use NGC 5194 and NGC 5195.

One reason for the continuing uncertainty about the M51 system is the lack of kinematic information for the companion galaxy. Unlike NGC 5194, NGC 5195 contains no neutral hydrogen, so the only kinematic data we have on NGC 5195 comes from measurements of the stellar kinematics of the system's inner disk (Schweizer 1977). Since tidal kinematics provide strong constraints for dynamical models of interacting galaxies (e.g., Hibbard & Mihos 1995), this dearth of information at large radii is a significant stumbling block for unraveling the evolutionary history of the system.

In principle, there is another dynamical tracer which can reveal the kinematic structure of M51's tidal debris — planetary nebulae (PNe). Since PNe are a normal and common phase of stellar evolution, their spatial distribution and kinematics closely follows that of the stellar component as a whole. As a result, surveys for PNe can trace the distribution of stars to lower surface densities than is possible with diffuse light. More importantly, PNe are extremely luminous emission-line sources. At the distance of M51 ($d = 8.4 \pm 0.6$ Mpc; FCJ), PNe surveys with 4-m class telescopes can reach ~ 2 mag down the planetary nebula luminosity function, and the velocity of each PN can be measured to ~ 10 km s^{-1} accuracy. This makes PNe uniquely useful as a kinematical probe of diffuse tidal structures, such as those found in the M51 system.

In 1997, FCJ surveyed M51 for planetary nebulae in order to obtain a distance to the system via the planetary nebula luminosity function. This survey found a substantial number of PNe directly west-southwest of NGC 5195 in a tidal tail-like structure. At first, this discovery was a bit of a surprise, since the deep broadband images of Burkhead (1978) place the western tail of NGC 5195 more to the northwest, and not at the location of these planetaries. However, numerical models (e.g.,Toomre 1994, as reported by Barnes 1998; Salo & Laurikainen 2000) do predict the presence of tidal material from NGC 5194 in the region where the planetaries are located.

In order to study this feature in more detail, and to provide kinematic data on the diffuse tidal structures surrounding M51, we have conducted a radial velocity survey of a significant fraction of the FCJ planetary nebula sample. The ultimate goal of these observations is to provide a more complete description of the kinematics of the M51 system, and test whether the kinematics of NGC 5195's tidal features are consistent with the extant models. Interestingly, our PN velocities reveal significant kinematic substructure in the diffuse material to the west of NGC 5195; this fact, combined with differences in the spatial distribution of the region's PNe and diffuse light, implies that the observed tidal tail consists of two distinct but overlapping features. We interpret these data in the light of published models and our own new N-body model.

The outline of our paper is as follows: in §2 we detail the original imaging and follow-up spectroscopic observations. In §3, we describe our data reduction and the determination of the planetary nebula velocities. In §4 and 5, we describe the kinematic structure of M51's western tidal tail, and compare the data to a new simulation which follows the response of both NGC 5194 and its companion. In §6, we describe two unusual objects whose properties are significantly different from the bulk of the planetaries, and discuss their implications. Finally, in §7, we summarize our results.

2. OBSERVATIONS

The detection of M51's planetary nebula candidates was reported in full in FCJ: here we briefly summarize their results. The original data were taken with the KPNO 4 m telescope and the T2KB detector. PN candidates were defined as point sources detected manually that were present on co-added images taken through a redshifted [O III] λ5007 filter (central wavelength 5017 Å, full-width-half-maximum 31 Å), but not present on similarly co-added frames taken through a broader (275 Å FWHM) off-band filter ($\lambda_c = 5300$ Å). Thus, at M51's systemic velocity (463 km s^{-1}; Schweizer 1977), the survey was sensitive to emission-line objects with $-750 < v < 1100$ km s^{-1}. In addition, all PN candidates had to be completely invisible on complementary R-band and Hα images; this requirement helped discriminate true PNe from compact H II regions and supernova remnants. A total of 64 PN candidates were detected in the survey; the location of these objects are displayed in the left panel of Figure 1. As the figure indicators, 45 of the candidate PNe project onto a tail-like structure to the west of NGC 5195. These PNe do not simply follow the low-surface brightness features seen in the deep image of Burkhead (1978); the PNe extend much further west of the galaxy. To illustrate this effect, the right panel of Figure 1 shows a logarithmic stretching of the FCJ off-band image, binned 5×5 pixels to enhance the faint tidal features.

Also of note in Figure 1 is the paucity of PN candidates in the visible disk of NGC 5194. As noted by FCJ, this is due to the high surface brightness of the spiral arms, and the confusion caused by the system's many line-emitting H II regions and supernova remnants. However, outside the disk, the FCJ survey is uniform and complete. FCJ confirmed this by adding artificial stars to the M51 onband frame and determining the completeness limit, where the rate of recovery begins to decline. The lack of PN candidates southeast and due west of NGC 5194 is real: there is an absence of stellar material in these regions.

2.1. *Improved Astrometry of M51's Planetaries*

In FCJ, astrometry of M51's PN candidates was performed using the positions of stars in the *Hubble Space Telescope* Guide Star Catalog (GSC; Lasker et al. 1990). Unfortunately, in most cases, the CCD images of these stars were saturated; this forced FCJ to derive their PN coordinates using a set of secondary standards measured on digitized images of the Palomar Sky Survey. Although the formal rms error of this procedure was 0.″49, a two-step process such as this is clearly susceptible to systematic error.

To reduce this error and maximize the signal-to-noise of our spectroscopy, we re-derived the astrometry for M51's PN candidates using the more precise and much higher density USNO-A 2.0 astrometric catalog (Monet et al. 1996; Monet 1998) and the FINDER astrometric package from IRAF[4]. The new coordinates, as well as the previously measured m_{5007}

[4] IRAF is distributed by the National Optical Astronomy Observatory, which is operated by the Association of Universities for Research in Astronomy, Inc., under cooperative agreement with the National Science Foundation.

magnitudes, are given in Table 1; the rms error of our astrometry is $0\farcs4$. Note that our PN positions are significantly different from those given by FCJ: not only is there a systematic offset between the GSC and USNO catalogs ($-3\farcs7$ in right ascension and $+0\farcs3$ in declination), but there are also noticeable position-dependent terms in the GSC-based astrometry. We attribute this difference to the very small number (13) of GSC stars available for the original astrometric measurements, and the complex spatial distortions of the old KPNO 4 m prime focus corrector (Jacoby et al. 1998).

2.2. *WIYN Spectroscopic Observations*

On UT 16 May 2001 we used the WIYN 3.5 m telescope to measure the radial velocities of 43 of M51's planetary nebula candidates. The specific instrument configuration consisted of the Hydra fiber positioner with $2''$ diameter red-sensitive fibers, the WIYN's telescope's bench spectrograph, and a 600 lines mm^{-1} grating blazed at $10\fdg1$ in first order. This setup yielded spectra covering the wavelength range between 4400 Å and 7200 Å at 2.8 Å (168 km s^{-1}) resolution with a 1.4 Å pixel^{-1} dispersion.

Our data were collected in two fiber setups, the first targeted for 29 PNe (plus 3 sky fibers), the second for 27 PNe (plus 3 sky fibers). The exposure times for these setups were 90 min (3×30 min) and 120 min (4×30 min), respectively. To provide a check on the repeatability of our measurements, 14 PN candidates were observed twice through different fibers. Five candidate PNe were not detected in our survey; we expect these were likely missed due to fiber positioning errors, poor astrometry, or low fiber throughput[5]. This left us with a total of 37 objects for further analysis.

The wavelength calibration for each spectrum was provided by a CuAr comparison arc taken immediately before each observation. In addition, to test our ability to centroid the weak lines of M51 PNe, we also obtained a set of CuAr arcs at two different exposures, 10 s and 60 s. By comparing measurements of weak arc lines (i.e., lines comparable in strength to the [O III] λ5007 emission feature of M51 PNe) to measurements of the same lines taken at six times the exposure level, we placed a limit on the internal errors associated with our velocity measurements. Our centroiding uncertainty was typically 0.1 to 0.15 pixels, or less than 0.1 of a resolution element. This implies an expected velocity error for our measurements of < 20 km s^{-1}.

3. DATA REDUCTION AND ANALYSIS

The individual Hydra images were first pre-processed (bias subtracted and flat-fielded) with the DOHYDRA routine within IRAF, and then averaged together with SCOMBINE. A dispersion relation for each spectrum was then obtained by fitting 14 bright spectral lines on the CuAr arc spectrum with a 4-th order spline; the resulting solution had a 0.02 Å rms error. Once this was done, the spectra of our three sky fibers were averaged and then subtracted from those of our program objects to create a sky-subtracted spectrum for each planetary. Finally, the spectra of the 14 objects observed with both setups were combined to increase their signal-to-noise.

After completing these reduction procedures, we examined each spectrum for the presence of an unresolved emission line at the approximate location of [O III] λ5007 at the redshift of the galaxies. Of the 42 PN candidates observed, 36 had this feature, and ~ 23 also showed evidence for the weaker [O III] line at λ4959. In addition, one PN candidate (observed with both setups) exhibited a single, broad (~ 350 km s^{-1} FWHM) emission feature; this object is probably a background object and is discussed in §6.1. Figure 2 displays the PN spectra in the wavelength region about [O III] λ5007.

Velocities were determined for the PN candidates by assuming the unresolved emission line near 5015 Å is, indeed, redshifted [O III] λ5007, and centroiding the line with the SPLOT routine in IRAF. To avoid degrading the signal-to-noise, these measurements were carried out on the spectra prior to sky subtraction; this makes absolutely no difference to the analysis, as the sky around 5000 Å in our spectra is completely negligible, and velocities derived before and after sky subtraction showed no measurable difference. The PN velocities, corrected for the Earth's motion about the Sun, are listed in Table 1. Table 1 also notes those PN candidates that were not detected in our survey. Note that the tabulated velocities are based entirely on the emission line at [O III] λ5007. Although the weaker lines of [O III] λ4959 and Hα were detected in a number of spectra, the signal-to-noise of these lines were too low for an accurate velocity measurement.

To confirm our identification of the λ5015 emission line as redshifted [O III] λ5007, we used the velocities of Table 1 to shift each spectrum back into its rest frame. We then scaled the spectra so that all the putative λ5007 lines had the same weight, and summed the data to create one single composite spectrum. This spectrum is displayed in Figure 3. The left-hand panel of the figure clearly shows both [O III] λ5007 and [O III] λ4959. Despite the fact that the system throughput is decreasing rapidly shortward of 5000 Å, the ratio of the two oxygen lines (3.2:1) is nearly identical to that expected from atomic physics (2.98; Storey & Zeippen 2000). This ratio confirms that virtually all the observed objects are emission line objects associated with M51 (see Freeman et al. 2000 for a similar analysis on Virgo cluster PN spectra). The presence of Hα and [N II] $\lambda\lambda 6548, 6584$ in the right hand panel of Figure 3 provides additional evidence for this interpretation. The relatively strong [N II] to Hα ratio (~ 0.7) may suggest a fairly high abundance in the stars associated with the PNe in M51, as was seen in M32 (Stasinska, Richer & McCall 1998).

To estimate the random uncertainty associated with our velocity measurements, we used the sub-sample of PNe observed with both Hydra setups. Fourteen PN were observed twice. Of these, 12 had their [O III] λ5007 emission detected in both setups, one was detected only in Setup 2, and one had a broad, asymmetrical emission line that was unsuitable for

[5] While it is strictly possible that some of these candidates were spurious detections (eg. cosmic rays), all candidates from FCJ were visually inspected and confirmed to be stellar, making this hypothesis unlikely.

the experiment. A comparison of the velocities derived from the individual spectra of the 12 objects appears in Table 2. In general, the agreement between the two setups is excellent: if we ignore the highly discrepant velocity difference for PN 11, the mean difference between Setup 1 and Setup 2 is 0 ± 4 km s^{-1}, and the dispersion is 12 km s^{-1}. Thus the velocity error in a single spectrum is 8 km s^{-1} if the measurements are completely uncorrelated; however, we expect this is not quite the case, and the true error will lie between 8 km s^{-1} and 12 km s^{-1}. We have adopted the upper limit of 12 km s^{-1} as the measurement error of our derived velocities.

Figure 4 shows the locations of the spectroscopically-measured PNe overlaid on the [O III] image of FCJ. The PN velocities are denoted by color. The most striking feature of the figure is the velocity structure of the low surface-brightness tail just west of NGC 5195. As the histogram of Figure 5 indicates, the distribution is distinctly bimodal. Two thirds of the PNe in this region have radial velocities greater than the systemic velocity of either galaxy in the interaction (463 km s^{-1} for NGC 5194; 600 km s^{-1} for NGC 5195; Schweizer 1977). Conversely, the velocities of the remaining PNe are at or below systemic velocity of NGC 5194. This bimodal behavior contrasts with the broad but generally unimodal velocity distribution exhibited by the PNe east of NGC 5195 and in the outer disk of NGC 5194; these objects generally have velocities somewhere between the two systemic velocities. Since no H I is present in the western tidal tail of M51, the bimodal distribution of Figure 5 is the first measurement of velocity substructure in the region.

4. THE KINEMATIC STRUCTURE OF THE WESTERN TAIL

The velocity field of the PNe of M51 is complex. This is particularly apparent in the western tail of NGC 5195, where one sees a multi-modal distribution of velocities. Figure 6 illustrates the velocity structure by displaying the distribution of PN velocities north of NGC 5194, along an east-west swath across the face of NGC 5195. Two things stand out in this figure. First, the velocity spread at any position is highly clumped; this implies that we are not simply viewing a single, kinematically hot component (i.e., a galaxy halo). Instead the data suggest the existence of multiple kinematically cold components which likely arise from different parent populations. The second feature of Figure 6 is the presence of a significant gradient in the PN velocities. Since this gradient is in the same sense as that observed for the stars in the inner disk of NGC 5195 (Schweizer 1977), the data suggest that the *bulk* of the observable PNe in this region come from NGC 5195 itself, rather than being captured or tidal debris from NGC 5194.

Comparing the spatial distribution and kinematics of M51's PNe to published dynamical models is somewhat difficult, because these studies either did not model the detailed response of the companion (e.g., Hernquist 1990, hereafter H90) or employed simple N-body models which did not capture the full dynamical evolution of the system (Toomre 1978; Salo & Laurikainen 2000). However, we can make some qualitative inferences based on the published models. Two broad classes of models exist: single passage models, like the original Toomre & Toomre (1972) model (later refined by H90), and multiple encounter models, like the one recently proposed by Salo & Laurikainen (2000, hereafter SL00). Both models can reproduce the overall morphology of the M51 system fairly well; the multiple passage model better describes some of the detailed HI kinematics of NGC 5194, but predicts a more complicated structure for the long HI tidal tail than is actually observed.

In terms of the PN population west of NGC 5195, both classes of models predict that material from NGC 5194's disk will be dispersed in this region.[6] In the multiple passage model, this material has been perturbed in the very recent ($\sim 10^8$ yr) past by the second passage of NGC 5195. As a result, the model predicts a higher radial velocity for the material than is produced by corresponding single passage models (for example, see Figure 4 in SL00). In second passage models, the velocities of the region range from 400 to 525 km s^{-1}, while in single passage models, the velocities are between 385 and 425 km s^{-1}.

Since the PN velocities west of NGC 5195 (315-480 km s^{-1}) lie between these two ranges, we cannot reliably discriminate between the two models. There is some hint of a blueward gradient towards the west in our PN data, and this is more consistent with the SL00 multiple passage model than a single passage model, but the small number of velocities makes this result tentative at best. Furthermore, it should be re-emphasized that the PN kinematics in the western tail of the system are truly bimodal: there is a complete 140 km s^{-1} gap between two kinematic components. While SL00 did not show the kinematic structure of the companion's tidal debris, it is hard to understand how the galaxy could undergo several close passages with NGC 5194 and still have its material exhibit such discrete segregation in velocity space.

5. MODELING THE KINEMATICS OF THE PLANETARY NEBULAE

Our PN observations do not explicitly rule out either class of model, but, as SL00 point out, there are a number of features which argue for a multiple passage model for M51. First, the kinematics of NGC 5194's H I tail and the apparent tidal bridge between NGC 5194 and 5195 are better fit by a multiple passage model than a single passage model. Second, single passage models imply that a long time has elapsed since perigalacticon; it is not clear whether the strength of NGC 5195's tidal features is consistent with this prediction. Finally, many single passage models have trouble reproducing the morphology of NGC 5194's northwestern tidal plume (which gives rise to the blueshifted PNe component in the system's western tail). For example, in the SL00 models, this tail extends to the northwest of NGC 5195 (see their Figure 1), while in the models of Toomre (1994, as reported by Barnes 1998), the tail has the correct orientation, but the mass ratio of the galaxy pair is a hefty 1:1. These various inconsistencies make it interesting to re-investigate the single passage scenario to see if we can construct a model that better matches the spatial and kinematical distribution of the

[6] While this material was not evident in the H90 simulations, that is likely due to the relatively small particle numbers used in the study.

tidal debris. We can do this by revisiting the H90 single passage simulation and explicitly including the response of the companion.

We began the simulation process by first defining the structure of each galaxy. The galaxies were constructed in the manner described by Hernquist (1993), and consisted of an exponential stellar disk, a central bulge, and a truncated isothermal halo. The mass ratio of the components was $M_d : M_b : M_h = 1 : 0.33 : 5.8$. The companion was identical to the primary, except scaled down in mass by a factor of $f = 1/2$. The size and circular velocity of the model was scaled by $f^{\frac{1}{2}}$ and $f^{\frac{1}{4}}$ respectively, which preserved disk surface density between the two models and provided a Tully-Fisher-like $M \sim V_c^4$ scaling of the model. The simulations were then evolved in a self-consistent manner using TREECODE (Hernquist 1987), using a total of $N = 55,296$ particles for the models which survey parameter space, and with a total of $N = 425,984$ particles (N_{disk}=131,072; N_{bulge}=16,384; N_{halo}=65,536 in each galaxy) for the final model. The simulations surveying parameter space were run using a parallel processing Beowulf cluster.

To begin the interaction modeling, we used the parameters of the self- consistent simulation of H90 as our starting point. These parameters include an NGC 5194/NGC 5195 mass ratio of 2:1, an initially parabolic orbit with a perigalacticon distance of 6 disk scale lengths, and a disk geometry for NGC 5194 of (i_1,ω_1)= (−70,−45), where i and ω are the orientation angles as defined by Toomre & Toomre (1972). After surveying simulations with varying ω_1 we settled on a value of $\omega_1 = 0$, which resulted in a longer and thinner tidal tail for NGC 5194 (as perigalacticon occurs in NGC 5194's disk plane) and kept the companion closer to NGC 5194 in projection while still preserving a fairly high projected velocity difference between the two galaxies.

With the parameters of NGC 5194's disk and relative orbit set in this manner, we next ran a grid of simulations covering the range of possible orientations (i_2, ω_2) for NGC 5195. To quickly narrow down the list of possible geometries, we examined the simulations to select those which gave the closest morphological match to the M51 system. In doing this, we paid particular attention to the tidal plumes northeast and southwest of NGC 5195. We were constrained in viewing geometry by the need to match the projected position and relative velocity of the galaxy pair, and by the observed 20° inclination of NGC 5194's disk (Tully 1974). NGC 5195's observed inclination also provided a constraint to the simulations. Based on the ellipticity of NGC 5195's isophotes, Schweizer (1977) inferred an inclination angle of 48° for the system. Although this estimate may be affected by tidal deformation, the galaxy's appreciable velocity gradient ($\sim$ 120 km s^{-1}; Schweizer 1977) requires that it not be too face-on. The final constraint on the models came from NGC 5195's rotation, which is east to west in the inner portions of the galaxy (Schweizer 1977). The models which best matched these morphological and kinematic requirements had geometries for the companion in the range of $(i_2, \omega_2) = (105 \pm 15, -30 \pm 15)$, with our favored model having $(i_2, \omega_2) = (110, -30)$.

An evolutionary sequence of our model is shown in Figure 7. The initial passage occurred 280 Myr ago, similar to H90's best match time of $\sim$ 300 Myrs past perigalacticon. At the present time (T=0), the galaxies are widely separated ($\Delta R \sim$ 50 kpc) and moving apart from one another quite rapidly ($\Delta V \sim$ 150 km/s; in other words, since NGC 5195 is behind NGC 5194 in our model, the observed radial velocity difference closely reflects the separation velocity). This is quite unlike the simulation of SL00, which favors a much closer true separation and an orbit which has carried the companion just past a second disk passage.

The model above plausibly reproduces the main morphological and kinematic properties of the M51 system, including the sharp northwestern tidal tail of NGC 5195. We now compare the tidal kinematics in the model against the kinematics of the planetary nebulae. To do this, we examined the projected velocity distribution of the model in the four regions of the system which contain the majority of our planetary nebulae. These regions are illustrated in Figure 8. Note that a strict comparison between the PNe and the model is not possible, since the selection criteria for the two datasets are very different: while the simulation samples velocities weighted by mass, the observational data suffer from constraints imposed by our non-random target selection and fiber crowding. Therefore, in order to compare the model to the PN velocities, our approach was to look more for similar patterns of kinematic substructure, rather than to perform a detailed one-to-one matching.

Field 1, which is immediately west of NGC 5195, has the most interesting velocity field. The stellar kinematics in this region are distinctly bimodal: there is a velocity peak at $v_r \sim 250$ km s^{-1} which corresponds to the tidal plume from NGC 5195, and a second peak around $v_r \sim -50$ km s^{-1}, which comes from material pulled out of NGC 5194. This echoes the distribution of PN velocities, and explains the existence of three blue-shifted PNe (relative to NGC 5195 systemic) just west of the body of NGC 5195: it is here that NGC 5194's tidal plume projects across the face of NGC 5195. The three other blue-shifted PNe further west and south of NGC 5195 are either with NGC 5194's plume or with the diffuse extension of the NGC 5194's disk. In either case, their velocities more closely reflect NGC 5194's systemic velocity rather than that of NGC 5195's tail. The model also has a clear gap in velocity between the two components; this results from the fact that these two tidal features are spatially distinct and kinematically cold.

Field 2 is east of the apparent tidal bridge which links NGC 5194 and NGC 5195. Like Field 1, this region, too, shows a multimodal velocity pattern, which arises from the discrete populations of NGC 5194's bridge and NGC 5195's eastern tidal tail. Unfortunately, our model for Field 2 does not match the PN velocity distribution very well: although there is a cluster of PNe near the predicted velocity of NGC 5195's tail, there are no blue-shifted PNe in our sample. Instead, the region contains two unexplained red-shifted PNe. This discrepancy is somewhat disturbing, but it hard to make a strong statement about the quality of the agreement based on only 5 objects. This is particularly true since our models do not account for the presence of kinematically hot populations (see §6.2 for further discussion on this point).

Fields 3 and 4 are much more straightforward to interpret. Field 3 covers the southwestern portion of NGC 5194's disk,

and Field 4 includes the northeastern portion of NGC 5195. In both fields, the model velocity distribution is single-peaked, and representative of the large scale velocity field of the superposed galaxy. The match with the PN velocities in Field 3 is excellent: both the velocity mean and the dispersion agree with the predictions of the model. The agreement of Field 4 is slightly worse, since the PNe there have slightly larger velocities than predicted. Of course, the prior constraints on the model – that the southern portion of M51 and the eastern portion of NGC 5195 both be blueshifted relative to their systemic velocities – practically ensures that the match between the model and the mean of the PN velocity distribution is close. However, the velocity dispersion of each field is also reproduced well by the model, which is not guaranteed by these velocity constraints.

While our model reproduces many of the morphological and kinematic features of the M51 system, there are still some discrepancies. Morphologically, NGC 5195's eastern tail seems to tilt slightly more south than it does in our model, and the apparent bridge between the modeled galaxies shows more curvature than is actually observed. Also, as the data of Field 1 and 4 indicate, our model predicts too large of a velocity gradient across NGC 5195. There are a number of ways to fix this problem, such as changing the orientation of NGC 5195's disk (i_2, ω_2) so that the system is observed more face-on, or reducing NGC 5195's mass (i.e., by using a 3:1 mass ratio for the system) and thus decreasing the galaxy's rotation velocity. However, our main goal here is to see whether a classic single passage model can reproduce the global morphology and kinematics of the tidal features of M51; clearly, this model presents such a solution.

Nevertheless, we leave with a cautionary note. Parameter space is wide, and the parameters describing the interaction are all tightly coupled. The morphology of tidal debris depends on the encounter geometry, the orbital parameters, the viewing angle and time, and the structural properties of the galaxies. For example, the dark matter distributions of NGC 5194 and NGC 5195 at large radius have a profound impact on the orbital evolution of the system. Since the viewing angle is constrained by the projected separation and velocity of the galaxy pair, the best-fitting value for this parameter will change if the dark matter distributions are modified. A different viewing angle will then alter the observed morphology of the system and the projected distribution of the tidal debris. Because of this degenerate coupling of parameters, iterating one parameter while holding the others fixed can be a misleading exercise and lead one to a "local minimum" in parameter space that ignores the much wider parameter space available. Simulations such as the one presented here should be viewed as caricatures of the real system, with broad uncertainties and lingering concerns about uniqueness.

With this in mind, we have no illusions that our model is the last word on the M51 solution. We have focused mainly on a comparison of the morphology, global kinematics, and PNe velocity field. Further revisions – and perhaps very different solutions – may be possible based on more detailed matching of the velocity field. Indeed, the multiple passage models of SL00 argue for a more tightly bound "second passage" encounter based on the detailed HI kinematics of the system, and may do an equally good job of modeling the PNe kinematics. However, it is unclear whether these second passage models can reproduce the bimodality *and* kinematic coldness of the distinct tidal features which comprise the western tail. Self- consistent simulations and detailed kinematics for these second passage models will be useful in testing these models; unfortunately, the uniqueness of these solutions will be even more questionable since they rely on the interplay between the (largely unconstrained) dark matter halos, dynamical friction, and orbital decay to obtain the best match for the M51 system.

6. UNUSUAL OBJECTS

There are two PNe candidates, PN 52 and PN 27 that are in clear disagreement with the dynamical model we have adopted. We now discuss these objects and attempt to determine their true nature.

6.1. *PN 52 - A Lyα galaxy?*

Figure 9 compares the optical spectrum of PN 52 to that of another PN in the survey. Photometrically, both objects are similar, with λ5007 fluxes of $\sim 1.1 \times 10^{-16}$ ergs cm^{-2} s^{-1}. However, as the figure illustrates, the two sources are different spectroscopically. First, PN 52 has no detectable [O III] λ4959 line – true planetary nebulae must have this line, and, as the comparison spectrum demonstrates, this line should have been seen. It was not[7], and, in fact, no other lines have been reliably detected in this spectrum. Second, the line profile of PN 52 is anomalously broad and asymmetric. The width of the object's lone emission line is approximately 6 Å (FWHM); for comparison, the spectrograph's instrumental profile is 3.0 Å(FWHM). No other PN in the sample has a resolved line. Finally, if we identify the emission line as [O III] λ5007, then the heliocentric velocity of the object is -176 km s^{-1}, or -640 km s^{-1} systemic. Such an object cannot be gravitationally bound to M51.

The most likely explanation for PN 52 is that it is not a planetary nebula at all, but a higher redshift source whose emission line has been red-shifted into FCJ's [O III] λ5007 filter. This is quite plausible: in a deep blank-field survey far away from any galaxy or cluster, Ciardullo et al. (2002) found a population of extragalactic sources that mimic the properties of planetary nebulae. If we scale the results of this survey to the area and depth of the M51 survey (256 arcmin^2, $m_{lim} = 26.3$) and the width of the narrow band filter, we should expect 0.8 ± 0.5 contaminating sources to be present in the FCJ sample.

PN 52 is not the first contaminating source to be found in a deep [O III] λ5007 planetary nebula survey. Some intracluster PN candidates in Virgo have turned out to be high-redshift objects (Kudritzki et al. 2000; Freeman et al.

[7] Although there is a hint of emission near λ4959, its centroid is 4 Å too blue for it to be the [O III] line.

2000). Also, in a recent PN survey of NGC 4697, Méndez et al. (2001) reported that three of his 535 PN candidates were interlopers. Based on these data, it is clear that some amount of contamination will be present in all [O III] λ5007 observations fainter than $m_{5007} = 26.0$. Future radial velocity surveys of PNe in external galaxies need to take this effect into account.

What is the true identity of PN 52? In order to be listed as a PN candidate by FCJ, the emission equivalent width must be extremely large, $\gtrsim 100$ Å. This, along with the object's asymmetric line profile, suggests that the source is a Lyα galaxy at redshift $z \sim 3.12$. We caution that this interpretation is not conclusive: Stern et al. (2000) have shown that lower redshift objects can masquerade as high-z Lyα emitters. To conclusively confirm the identity of this object, deeper spectroscopy is needed, to either detect the Lyman decrement or find additional emission lines in the spectrum.

6.2. *PN 27 - A highly blueshifted PN*

Spectroscopically, PN 27 is very similar to the other PNe surveyed in this program: its [O III] λ5007 emission line is strong and unresolved, and the weaker [O III] λ4959 line is present at roughly 1/3 the strength of λ5007. However, in terms of location and motion, the object is unique. PN 27 sits SSE of M51 well away from any extended tidal plume (see Figure 1, left), and it has a radial velocity of 194 km s^{-1}. In other words, PN 27 is blue-shifted by 269 km s^{-1} relative to NGC 5194, and 406 km s^{-1} relative to NGC 5195. This remarkable velocity is not due to measurement error. PN 27 was observed twice: in both cases, both lines of [O III] were detected. The velocity difference between the two measurements is only 3 km s^{-1}.

If PN 27 belongs to NGC 5194, then it is moving at -269 km s^{-1} with respect to NGC 5194. What can cause this motion? One possibility is that PN 27 belongs to the stellar halo of the galaxy. In the Milky Way, such high-velocity objects do exist, as the vertical velocity dispersion in the spheroidal component is $\gtrsim 100$ km s^{-1} (Mihalas & Binney 1981). If the stellar halo of NGC 5194 is similar to that of the Milky Way, then it is at least conceivable that a high velocity PNe could have been observed.

We can estimate how likely the halo PN explanation is by using the bulge/disk parameters for NGC 5194 given by Baggett, Baggett, & Anderson (1998). As column (4) of Table 1 demonstrates, the FCJ survey of NGC 5194 was restricted to galactocentric radii $2\farcm8 \lesssim R_{\rm iso} \lesssim 8\farcm0$. If we extrapolate the Baggett et al. $r^{1/4}$-law to these radii, adopt the FCJ distance of ~ 8.4 Mpc, and apply the bolometric correction of an old population (-0.8; Jacoby, Ciardullo, & Ford 1990), then we obtain a value of $L_{\rm bol} \sim 2 \times 10^9 L_\odot$ for the amount of spheroid (bulge+halo) luminosity contained in the FCJ survey field. To translate this into an expected number of PNe, we assume old stellar populations produce $\sim 20 \times 10^{-9}$ PNe (within 2.5 mag of the luminosity function cutoff, M^*) per unit bolometric luminosity (Ciardullo 1995). When we scale this to the FCJ survey depth (1.2 mag down the PN luminosity function), we get a value of ~ 14 for the number of spheroid PNe that could have been detected. Since we obtained spectroscopy for roughly half of the FCJ planetary nebula candidates, the result is that we might expect ~ 7 spheroid PNe to be present in our sample.

Of course, not all halo objects have large vertical velocities. For example, of the 95 probable Milky Way halo RR Lyrae stars studied by Layden (1995), only two have a vertical velocity as great as 269 km s^{-1}. If the spheroidal component of M51 is similar to that of the Milky Way, then the probability of finding a high-velocity PN in our sample is small, ~ 0.1. This number is highly uncertain, as it is derived from a rather large photometric extrapolation and an assumed 'maximal' $r^{1/4}$ spheroid. Nevertheless, it does demonstrate that the presence of halo PNe in our sample is possible.[8] Such a 'hot' population was not explicitly included in our models.

An alternative explanation for the high velocity of PN 27 is that it is a 'runaway star', where the ejected planetary obtained a high velocity from either the tidal interaction (e.g., Byrd 1979), or from some other dynamical process. However, we believe this hypothesis to be less likely – our dynamical models show no evidence for an extremely blueshifted population, and none of the hypothesized models for high-velocity neutron stars (e.g., Cordes & Chernoff 1998), or O & B stars seem relevant in this case.

The best way to distinguish between these two scenarios is through deeper PN spectroscopy. If the halo hypothesis is correct, we might expect PN 27 (and a few other objects) to have a sub-solar oxygen abundance and perhaps enhanced ratios of C/O and N/O; such properties have been observed for halo PNe in the Milky Way (Howard, Henry, & McCartney 1997). Deeper spectroscopy is also desirable for an improved kinematic model of the system. If the metallicities of the PNe could be derived, this information could be used to constrain the place of origin of individual objects.

7. SUMMARY

We have presented the velocities of 36 PNe in the interacting galaxy system M51. The planetaries have a velocity structure that is clearly multi-modal and complex, especially in the tidal debris west of the companion galaxy NGC 5195. In this region, we find two distinct kinematic components, consistent with the idea that we are viewing two tidal features – one from each galaxy – cospatially in projection. Such features have been predicted by numerical simulations (e.g., Salo & Laurikainen 2000), but the component from NGC 5194 has remained undetected until now. The PN kinematics do not yet discriminate between the various dynamical scenarios for the M51 system: both single- and multiple-passage models predict multiple kinematic features in this region. We do, however, note that the kinematic *coldness* of these features may be difficult to reproduce in a multiple passage scenario, where the galaxies have experienced several perturbative events. Self-consistent dynamical models of the multiple passage scenario are needed to test this effect. We expand on the previous

[8] As suggested in §5, a small number of our PN have velocities that do not agree with the model predictions. It is possible that these objects are also halo PNe.

simulation of Hernquist (1990) and present a new single-passage model that reasonably reproduces the morphology and kinematics of the system's tidal debris.

How can we better constrain the dynamical evolution of the M51 system? Observationally, the FCJ survey of M51 probed only the first 1.2 mag of the planetary nebulae luminosity function. The sample of 64 PNe found in this survey could easily be increased by a factor of ~ 3 by going deeper with current 4 m and 8 m class telescopes. There are roughly 10 PNe in an 18 arcmin^{-2} area in the FCJ sample of the northwestern tidal tail. Assuming roughly $\sim 20 \times 10^{-9}$ PNe per bolometric solar luminosity (2.5 mag down the PNLF) for a stellar population (e.g., Ciardullo 1995), and a distance of 8.4 Mpc, this PNe density translates to a stellar surface brightness of $\mu_V \sim 24.5$ mag arcsec^{-2}. Allowing for a 3-fold increase in the number of PNe detected in deeper surveys, and adopting a (conservative) minimum of 10 PNe in a given region to derive useful kinematic information, PNe could be used to probe surface brightnesses as faint as $\mu_V \sim 26$ mag arcsec^{-2}. The kinematics of such low-surface brightness features cannot be measured in any other way.

In addition to a deeper M51 PNe survey, more information on the secondary, NGC 5195, would be extremely helpful. In particular, integral-field spectroscopy (e.g., Andersen & Bershady 1999) of the galaxy's stellar component could dramatically improve our constraints on galactic rotation and inclination angle. Finally, better theoretical models are needed to predict the detailed tidal kinematics probed by the PNe. This is particularly true for the multiple-passage models, for which no fully self-consistent solution has yet been developed.

We thank the observing staff at the WIYN telescope, especially Di Harmer, for assisting us in obtaining excellent data. We also thank Paul Harding for useful discussions. This work was supported by the NSF through grants AST-9876143 (JCM) and AST 0071238 (RC) and through a Research Corporation Cottrell Scholarship (JCM).

REFERENCES

Andersen, D.R. & Bershady, M.A. 1999, ASP Conf. Ser. 182: Galaxy Dynamics - A Rutgers Symposium, eds. D.R. Merritt, M. Valluri, & J.A. Sellwood (San Francisco: ASP), 215
Baggett, W.E., Baggett, S.M., & Anderson, K.S.J. 1998, AJ, 116, 1626
Barnes, J.E. 1998, Saas-Fee Advanced Course 26: Galaxies: Interactions and Induced Star Formation, eds R.C. Kennicutt et al. (Berlin:Springer-Verlag), 275
Burkhead, M.S. 1978, ApJS, 38 147
Byrd, G.G. 1979, ApJ, 234, 481
Ciardullo, R. 1995, in I.A.U. Highlights of Astronomy 10, ed. I. Appenzeller (Dordrecht: Kluwer), 507
Ciardullo, R., Jacoby, G.H., & Dejonghe, H.B. 1993, ApJ, 414, 454
Ciardullo, R., Feldmeier, J.J., Jacoby, G.H., de Naray, R.K., Laychak, M.B., & Durrell, P.R. 2002, ApJ, in press
Ciardullo, R., Feldmeier, J.J., Krelove, K., Jacoby, G.H., & Gronwall, C. 2002, ApJ, 566, 784
Cordes, J.M., & Chernoff, D.F. 1998, ApJ, 505, 315
Dopita, M.A., Jacoby, G.H., & Vassiliadis, E. 1992, ApJ, 389, 27
Feldmeier, J.J. 2000, Ph.D. thesis, The Pennsylvania State University
Feldmeier, J.J., Ciardullo, R., & Jacoby, G.H. 1997 ApJ, 479, 231 (FCJ)
Freeman, K.C., Arnaboldi, M., Capaccioli, M., Ciardullo, R., Feldmeier, J., Ford, H., Gerhard, O., Kudritzki, R., Jacoby, G., Méndez, R.H., & Sharples, R. 2000, in ASP Conf. Ser. #197, Dynamics of Galaxies: From the Early Universe to the Present, eds. F. Combes, G.A. Mamon, & V. Charmandaris (San Francisco, Astronomical Society of the Pacific), 389
Hernquist, L. 1987, ApJS, 64, 715
Hernquist, L. 1990, in Dynamics and Interactions of Galaxies, ed. R. Wielen (Berlin: Springer-Verlag), 108 (H90)
Hernquist, L. 1993, ApJS, 86, 389
Hibbard, J.E., & Mihos, J.C. 1995, AJ, 110, 140
Howard, J.W., Henry, R.B.C., & McCartney, S. 1997, MNRAS, 284, 465
Howard, S., & Byrd, G.G. 1990, AJ, 99, 1798
Jacoby, G.H., Ciardullo, R., & Ford, H.C. 1990, ApJ, 356, 332
Jacoby, G.H., Liang, M., Vaughn, D., Reed, R., & Armandroff, T. 1998, Proc. SPIE, 3355, 721
Kudritzki, R.-P., Méndez, R.H., Feldmeier, J.J., Ciardullo, R., Jacoby, G.H., Freeman, K.C., Arnaboldi, M., Capaccioli, M., Gerhard, O., & Ford, H.C. 2000, ApJ, 536, 19
Lasker, B.M., Sturch, C.R., McLean, B.J., Russell, J.L., Jenkner, H., & Shara, M.M. 1990, AJ, 99, 2019
Layden, A.C. 1995, AJ, 110, 2288
Méndez, R.H., Riffeser, A., Kudritzki, R.-P., Matthias, M., Freeman, K.C., Arnaboldi, M., Capaccioli, M., & Gerhard, O.E. 2001, ApJ, 563, 135
Mihalas, D., & Binney, J. 1981, Galactic Astronomy (New York: Freeman)
Monet, D. 1998, BAAS, 30, 1427
Monet, D., Bird, A., Canzian, B., Harris, H., Reid, N., Rhodes, A., Sell, S., Ables, H., Dahn, C., Guetter, H., Henden, A., Leggett, S., Levinson, H., Luginbuhl, C., Martini, J., Monet, A., Pier, J., Riepe, B., Stone, R., Vrba, F., & Walker, R. 1996, USNO A - 1.0 A Catalog of Astrometric Standards, U.S. Naval Observatory, Washington, D.C.
Richer, M.G. 1993, ApJ, 415, 240
Rosse, W.P. 1845, June Meeting of the British Association for the Advancement of Science
Rosse, C. P. 1880, Transactions Royal Dublin Society, vol ii
Rots, A.H., Crane, P.C., Bosma, A., Athanassoula, E., & van der Hulst, J.M. 1990, AJ, 100, 387
Salo, H., & Laurikainen, E. 2000, MNRAS, 319, 377 (SL00)
Schweizer, F. 1977, ApJ, 211, 324
Scoville, N., & Young, J.S. 1983, ApJ, 265, 148
Stasińska, G., Richer, M.G. & McCall, M.L. 1998, A&A, 336, 667
Stern, D., Bunker, A., Spinrad, H., & Dey, A. 2000, ApJ, 537, 73
Storey, P.J., & Zeippen, C.J. 2000, MNRAS, 312, 813
Toomre, A. 1978, in IAU Symp. 79, Large Scale Structures in the Universe, ed. M.S. Longair & J. Einasto (Dordrecht: Reidel), 109
Toomre, A., & Toomre, J. 1972, ApJ, 178, 623
Tully, R.B. 1974, ApJS, 27, 449
Zaritsky, D., Rix, H., & Rieke, M. 1993, Nature, 364, 313
Zwicky, F. 1959, Hdb. d. Phys. 53, 373

TABLE 1
M51 PLANETARY NEBULA CANDIDATES

ID	α(2000)	δ(2000)	$R_{\rm iso}$ (arcmin)	m_{5007}	Velocity (km s^{-1})	Notes[a]
1	13 29 50.61	+47 06 27.5	5.3	25.15	535	S
2	13 30 03.73	+47 17 57.3	6.5	25.34	657	S
3	13 30 16.82	+47 14 01.8	4.7	25.35	657	S
4	13 29 38.52	+47 17 38.2	6.4	25.36	724	S,T
5	13 29 23.33	+47 17 25.3	7.6	25.38	664	S,T
6	13 29 44.86	+47 09 15.0	2.8	25.38	522	
7	13 29 29.37	+47 15 11.1	5.3	25.39	406	S,T
8	13 29 48.90	+47 16 37.6	5.0	25.42	476	S,T
9	13 30 14.89	+47 14 43.4	4.8	25.44	500	S
10	13 29 48.95	+47 17 21.6	5.7	25.48	432	S,T
11	13 29 57.33	+47 17 29.0	5.9	25.51	704	T
12	13 29 38.99	+47 08 05.0	4.3	25.52	488	
13	13 29 37.28	+47 17 25.9	6.3	25.54	713	S,T
14	13 29 29.07	+47 17 19.7	6.9	25.55	736	S,T
15	13 29 35.89	+47 16 42.0	5.8	25.55	655	S,T
16	13 29 36.65	+47 07 07.0	5.3	25.62	448	S
17	13 29 48.04	+47 15 57.8	4.3	25.62	687	S,T
18	13 29 49.23	+47 17 23.5	5.7	25.62		S,T
19	13 30 00.56	+47 17 08.3	5.6	25.63	...	N,T
20	13 29 50.36	+47 17 11.9	5.5	25.65		S,T
21	13 29 36.93	+47 08 35.0	4.1	25.66	511	
22	13 29 34.49	+47 17 38.9	6.7	25.66		S,T
23	13 29 46.61	+47 17 10.3	5.6	25.68	413	T
24	13 29 46.03	+47 15 31.2	4.0	25.68		S,T
25	13 29 31.22	+47 15 47.2	5.5	25.68	430	S,T
26	13 29 30.08	+47 16 31.3	6.2	25.68	629	S,T
27	13 30 05.70	+47 07 19.4	4.9	25.69	194	S
28	13 29 42.63	+47 18 18.5	6.8	25.70	745	S,T
29	13 29 40.21	+47 15 12.8	4.1	25.70	692	S,T
30	13 29 40.95	+47 09 05.8	3.3	25.74	576	
31	13 30 00.01	+47 16 57.5	5.4	25.77		T
32	13 29 42.68	+47 18 52.2	7.4	25.81	...	N,S,T
33	13 30 01.11	+47 04 48.9	7.1	25.83	478	S
34	13 29 55.15	+47 18 29.1	6.8	25.85		S,T
35	13 30 07.93	+47 16 22.0	5.3	25.86	...	N,T
36	13 29 44.02	+47 16 13.7	4.8	25.88	...	N,S,T
37	13 29 30.87	+47 14 36.1	4.7	25.90	315	S,T
38	13 29 51.23	+47 16 05.9	4.4	25.93		T
39	13 29 45.83	+47 17 29.0	5.9	25.97		T
40	13 29 17.44	+47 15 21.5	7.0	25.98		S,T
41	13 30 05.40	+47 17 36.1	6.3	26.00		S,T
42	13 29 48.52	+47 17 18.1	5.7	26.00		T
43	13 30 12.65	+47 14 08.0	4.2	26.00	508	S
44	13 29 46.53	+47 06 54.4	4.9	26.02	534	S
45	13 29 43.93	+47 15 48.6	4.4	26.03		T
46	13 30 08.25	+47 16 18.8	5.3	26.03	515	
47	13 29 50.41	+47 05 38.7	6.1	26.08		S
48	13 29 24.23	+47 15 02.7	5.9	26.08		S,T
49	13 29 53.17	+47 05 44.9	6.0	26.09		S
50	13 29 44.80	+47 16 04.5	4.6	26.15		S,T
51	13 29 51.33	+47 18 33.7	6.9	26.16	692	S,T
52	13 29 16.27	+47 13 00.7	6.3	26.17	—	G,S,T
53	13 29 51.12	+47 17 19.7	5.7	26.17		
54	13 29 55.45	+47 18 57.7	7.3	26.21		T
55	13 29 54.70	+47 16 20.0	4.7	26.24		T
56	13 29 23.58	+47 17 13.6	7.4	26.26		S,T
57	13 30 08.28	+47 17 52.7	6.8	26.28	593	S
58	13 29 44.01	+47 05 51.9	6.0	26.29	...	N,S
59	13 29 46.96	+47 05 36.3	6.2	26.35		
60	13 29 45.44	+47 06 34.5	5.3	26.37	532	
61	13 30 33.91	+47 13 32.3	7.2	26.39	481	
62	13 30 11.08	+47 17 10.7	6.3	26.44	561	
63	13 29 26.01	+47 17 11.3	7.1	26.47		T
64	13 30 20.00	+47 13 09.1	4.8	26.94	607	

[a]G: object is probably a background Lyα galaxy (see §6.1 for details); N: no emission line detected; S: part of the FCJ statistical sub-sample used to derive the system's distance; T: planetary is west of NGC 5195 in a tidal tail.

TABLE 2
VELOCITY ERRORS

ID	Velocity (km s^{-1}) Setup 1	Setup 2	Δv (km s^{-1})
1	527	539	−13
3	661	654	+7
5	665	664	+1
11	674	720	−46
25	431	428	+3
27	194	191	+3
29	680	698	−19
33	477	479	−2
37	316	321	−6
51	689	693	−5
61	493	469	+24
64	610	601	+9

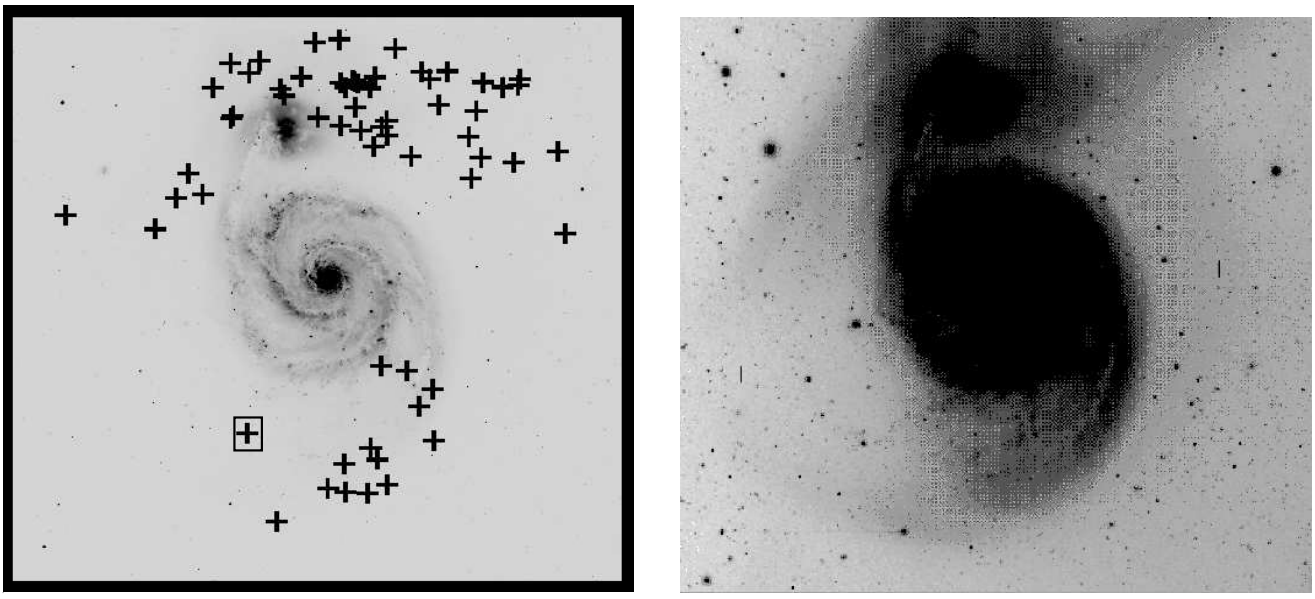

FIG. 1.— The left panel displays the [O III] λ5007 image of M51 taken by Feldmeier, Ciardullo, & Jacoby (1997). North is up and east is to the left; the image is $16' \times 16'$ in size. The positions of 64 planetary nebulae are denoted by crosses; the high-velocity PN 27 is identified by a box. On the right is the corresponding off-band image, binned 5×5 and logarithmically stretched to bring out low surface brightness features. The tidal features described by Zwicky (1959) and Burkhead (1978) are easily seen. Note that the planetary nebulae in the western tail follow a different morphology from the diffuse light.

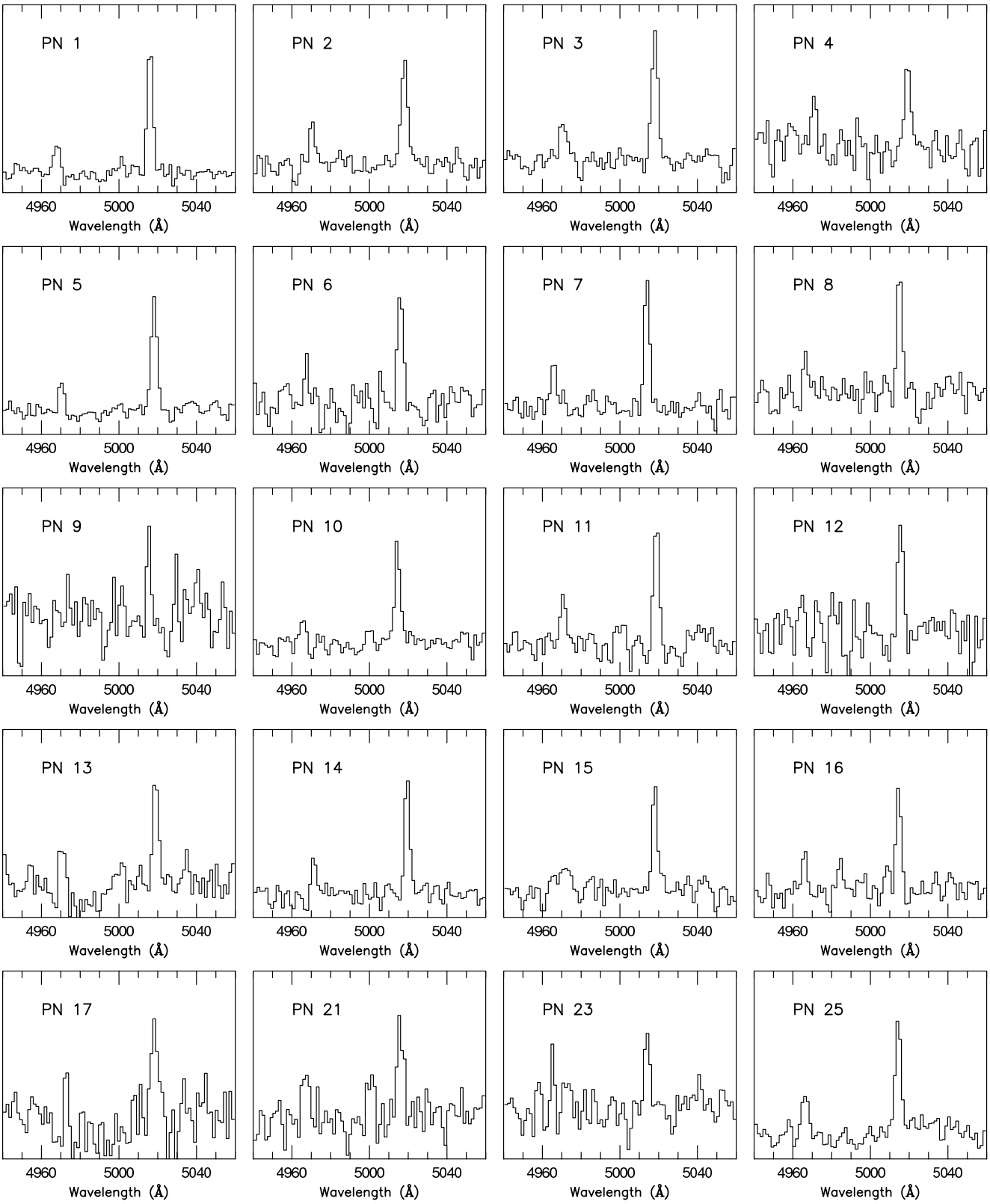

FIG. 2(A).— The sky-subtracted spectra of PN candidates 1 through 25 taken with the 3.5 m WIYN telescope. Only the wavelength region between 4940 and 5060 Å is shown; the vertical intensity scale is arbitrary. [O III] λ5007 is clearly visible in each spectrum; [O III] λ4959 is also often visible.

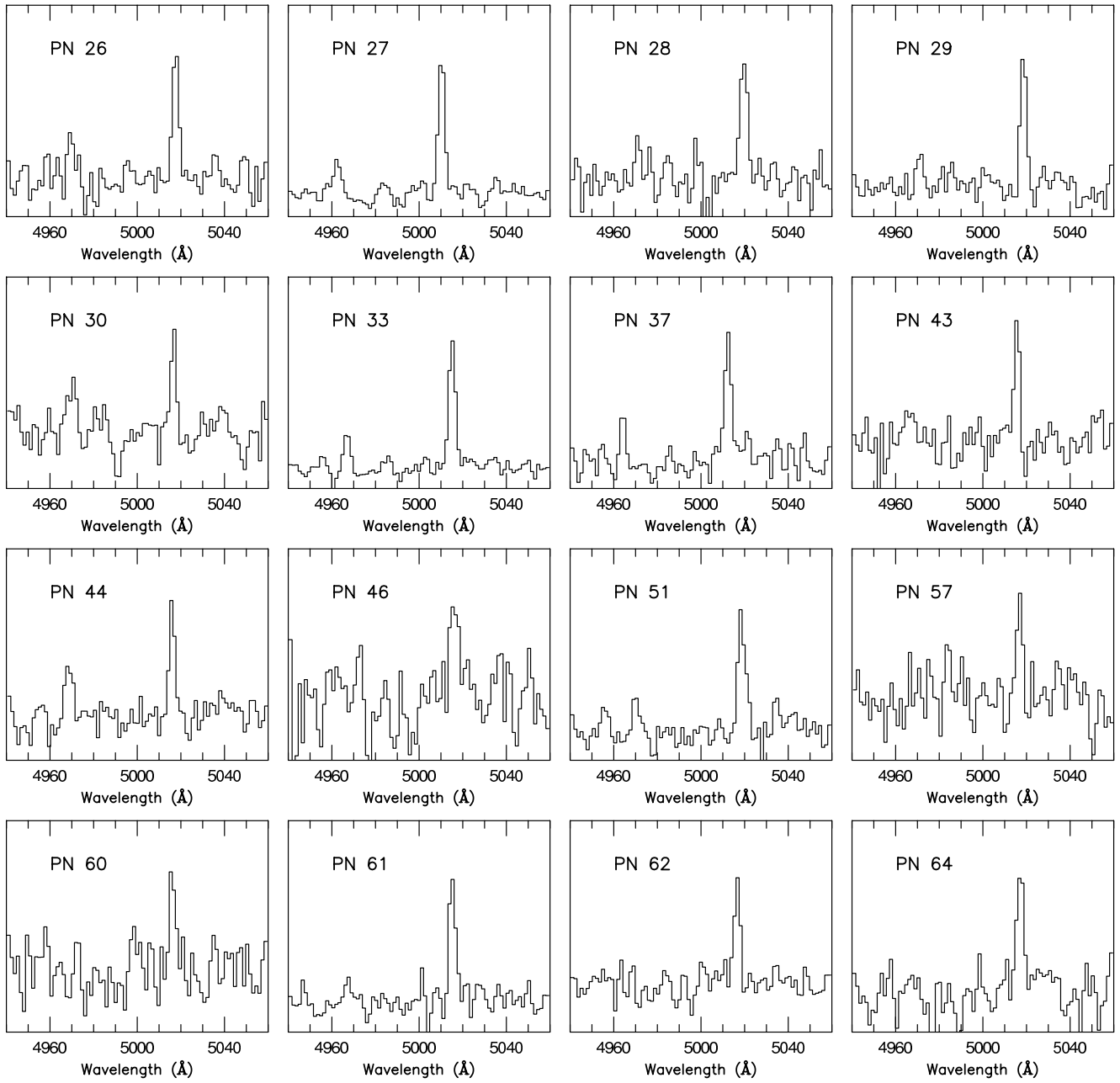

FIG. 2(B).— As in Figure 2(a), but for PN candidates 26 through 64.

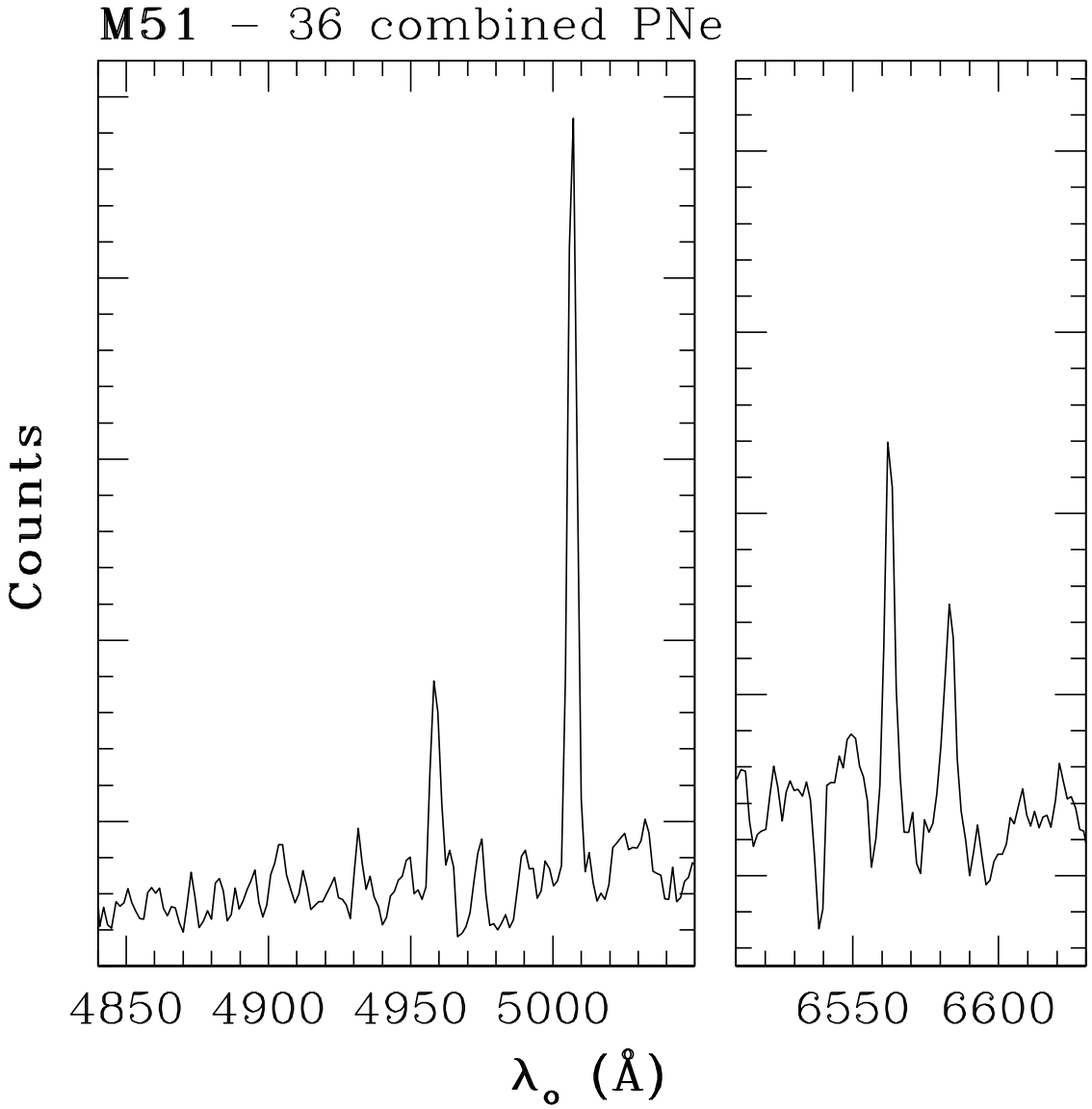

FIG. 3.— The co-added sky-subtracted spectra of the 36 candidate M51 PNe, as described in the text. The left panel shows the region about [O III] λ5007; the right panel displays the region near Hα. As expected for bona-fide planetary nebulae, the [O III] λ4959 line is clearly visible. The [N II] $\lambda\lambda 6548, 6584$ doublet is also seen, but the rapid decrease in system thoughput shortward of 5000 Å prevents us from seeing Hβ. The presence of these lines confirms that the observed objects are genuine planetary nebulae.

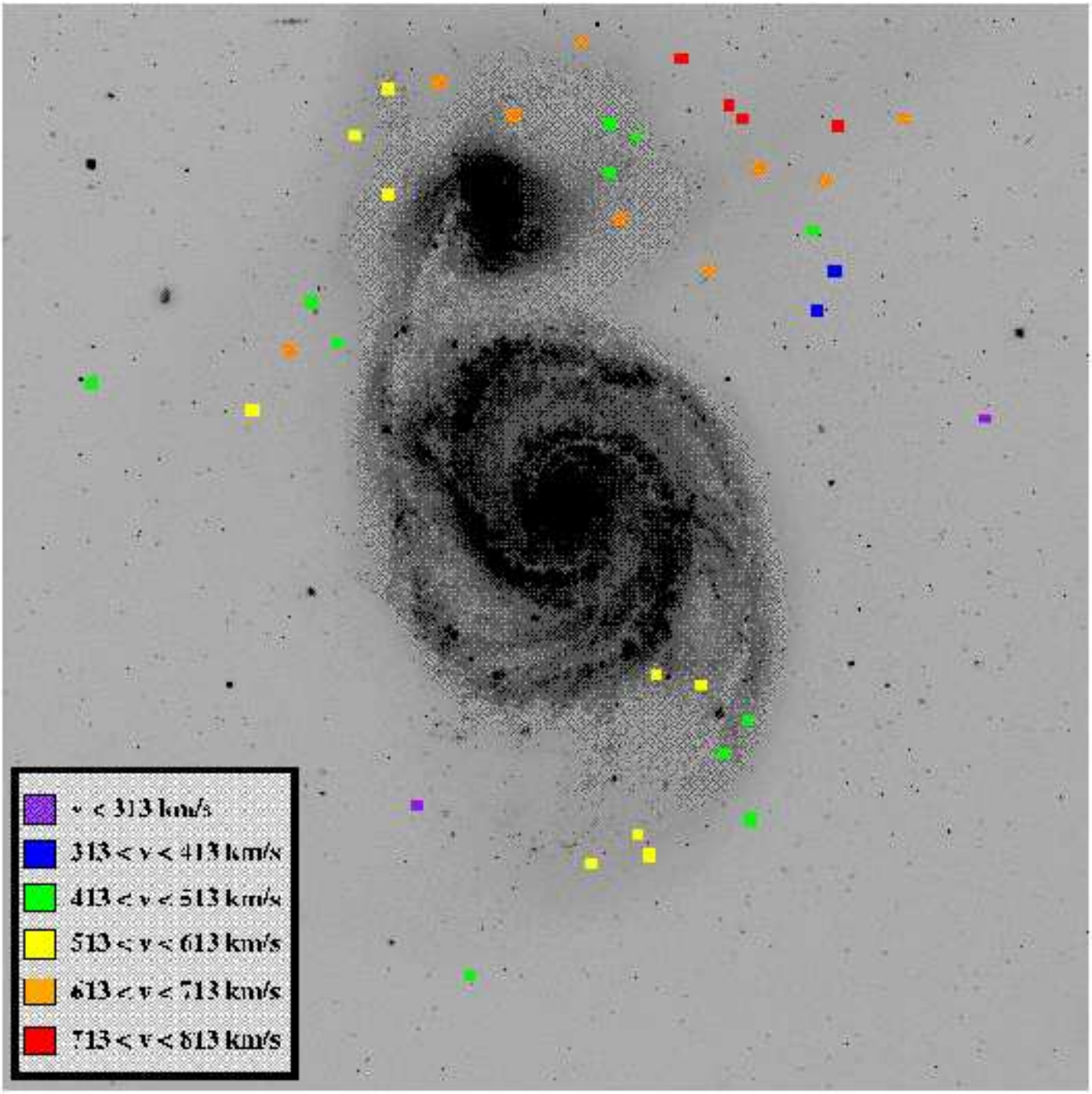

FIG. 4.— The locations of our spectroscopically confirmed PNe superposed on the FCJ [O III] λ5007 image of M51. North is up, and east is to the left; the image is $16'$ on a side. The PNe are color-coded by their heliocentric radial velocity. Note that the tidal tail structure west of NGC 5195 has multiple velocity components.

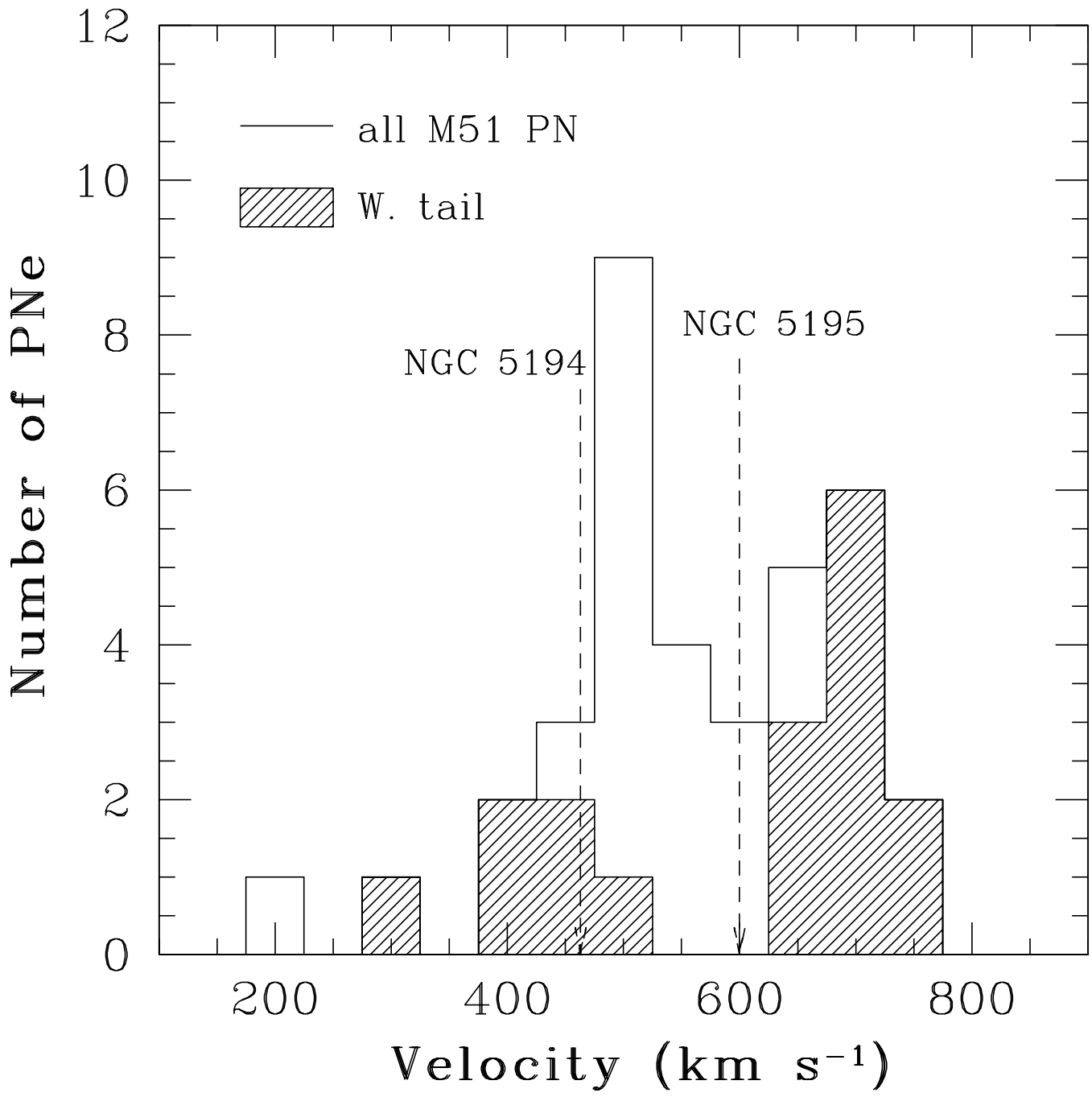

FIG. 5.— A histogram of the heliocentric velocities of PNe in the M51 system. The hatched region denotes PNe that are located in the western tail of NGC 5195; see text for details. The mean heliocentric velocities for the two galaxies (463 km s^{-1} for NGC 5194, 600 km s^{-1} for NGC 5195) are noted.

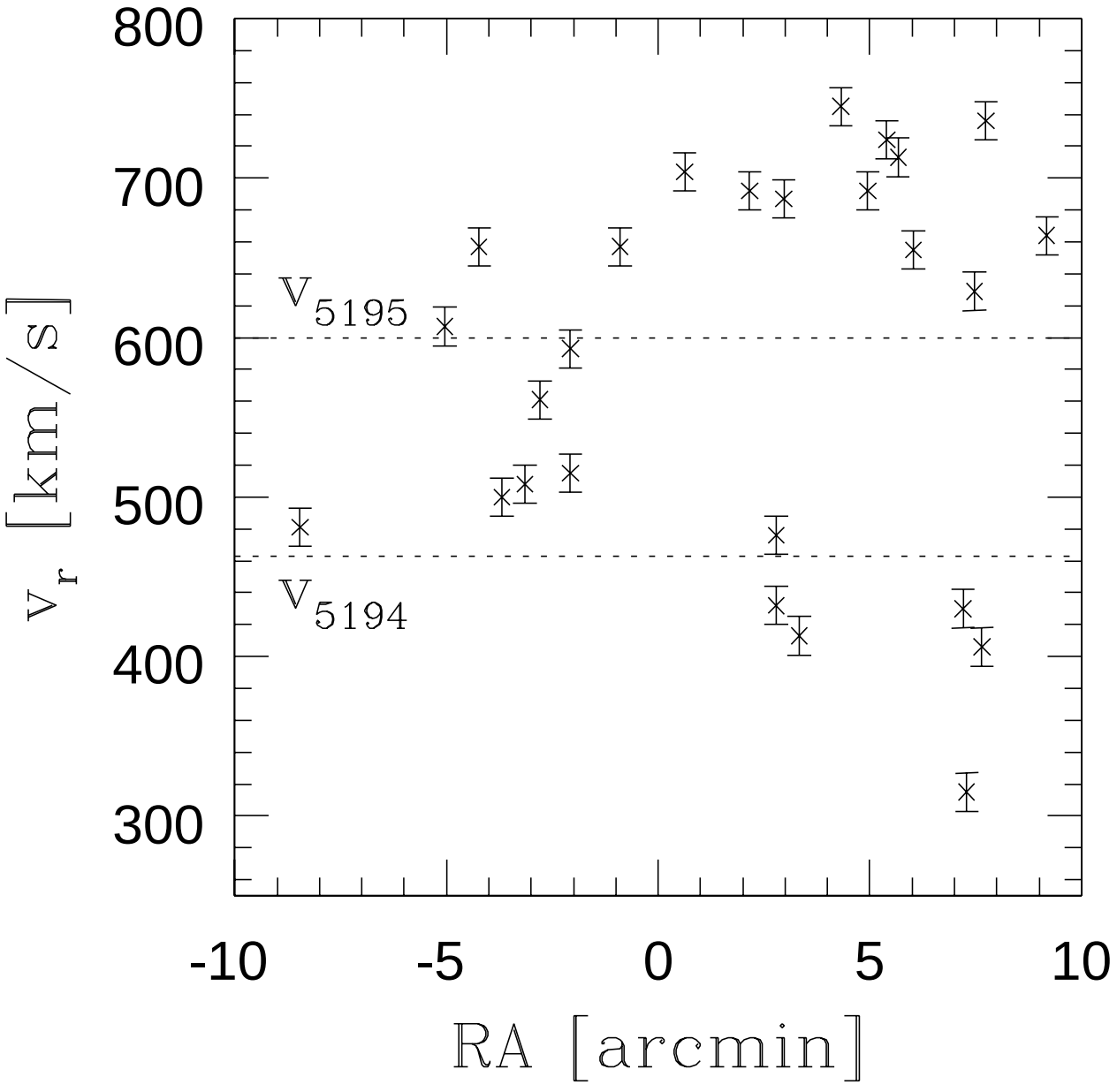

FIG. 6.— The velocities of planetary nebulae around NGC 5195, plotted as a function of right ascension. The spatial zeropoint is the position of NGC 5195's nucleus. Multiple dynamically cold components can be seen in the data. The bimodal kinematics of the western tail is obvious.

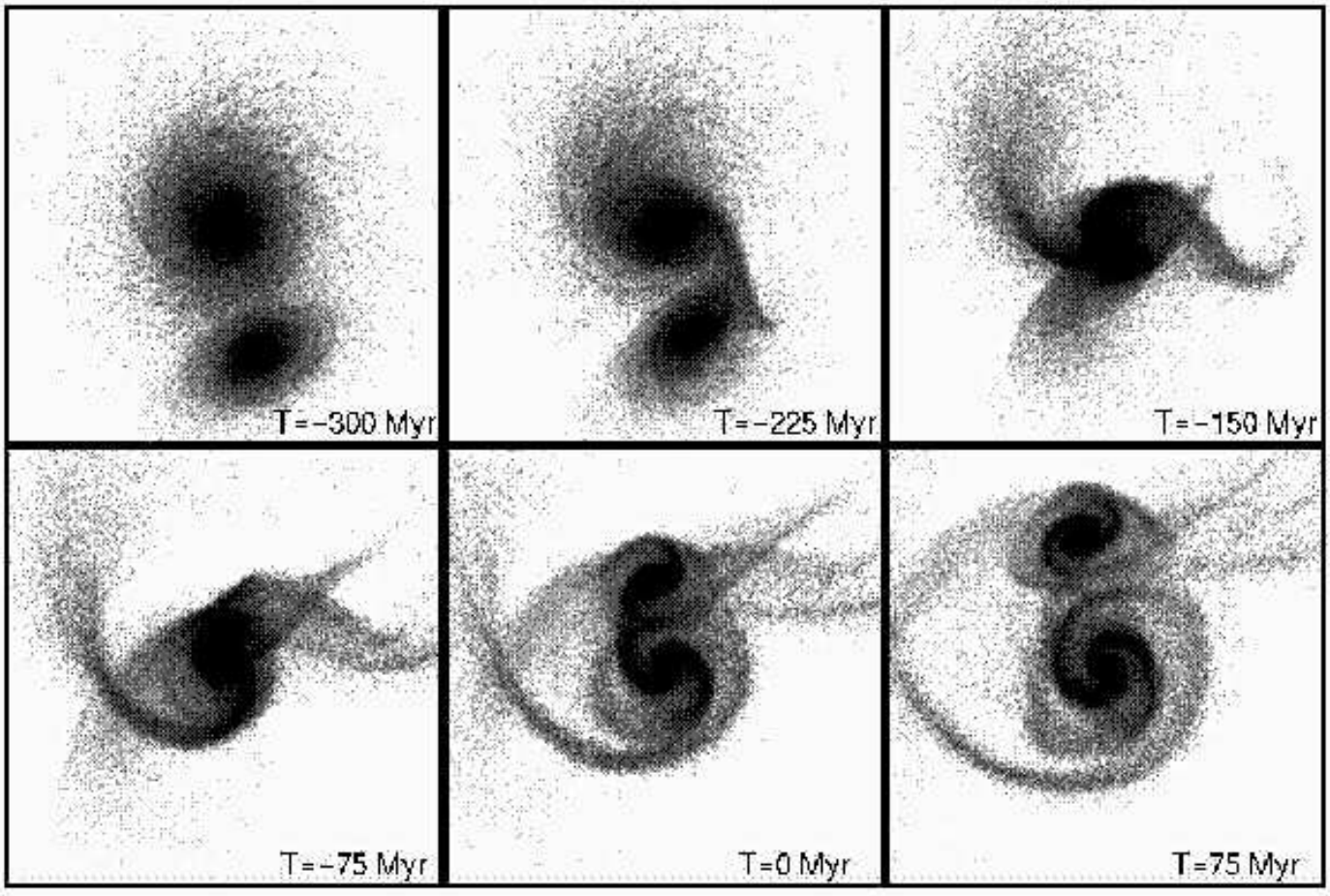

FIG. 7.— Time evolution of our new "single passage" model, shown projected onto the sky plane. Time is shown in the bottom right corner of each panel; T=0 corresponds to our best match viewing time. The sequence starts just before perigalacticon (which occurs at T=-280 Myr), after which the secondary galaxy, NGC 5195, passes behind the primary galaxy NGC 5194. At the current time, T=0, the "western tail" can be seen to contain tidal material from both galaxies seen in projection.

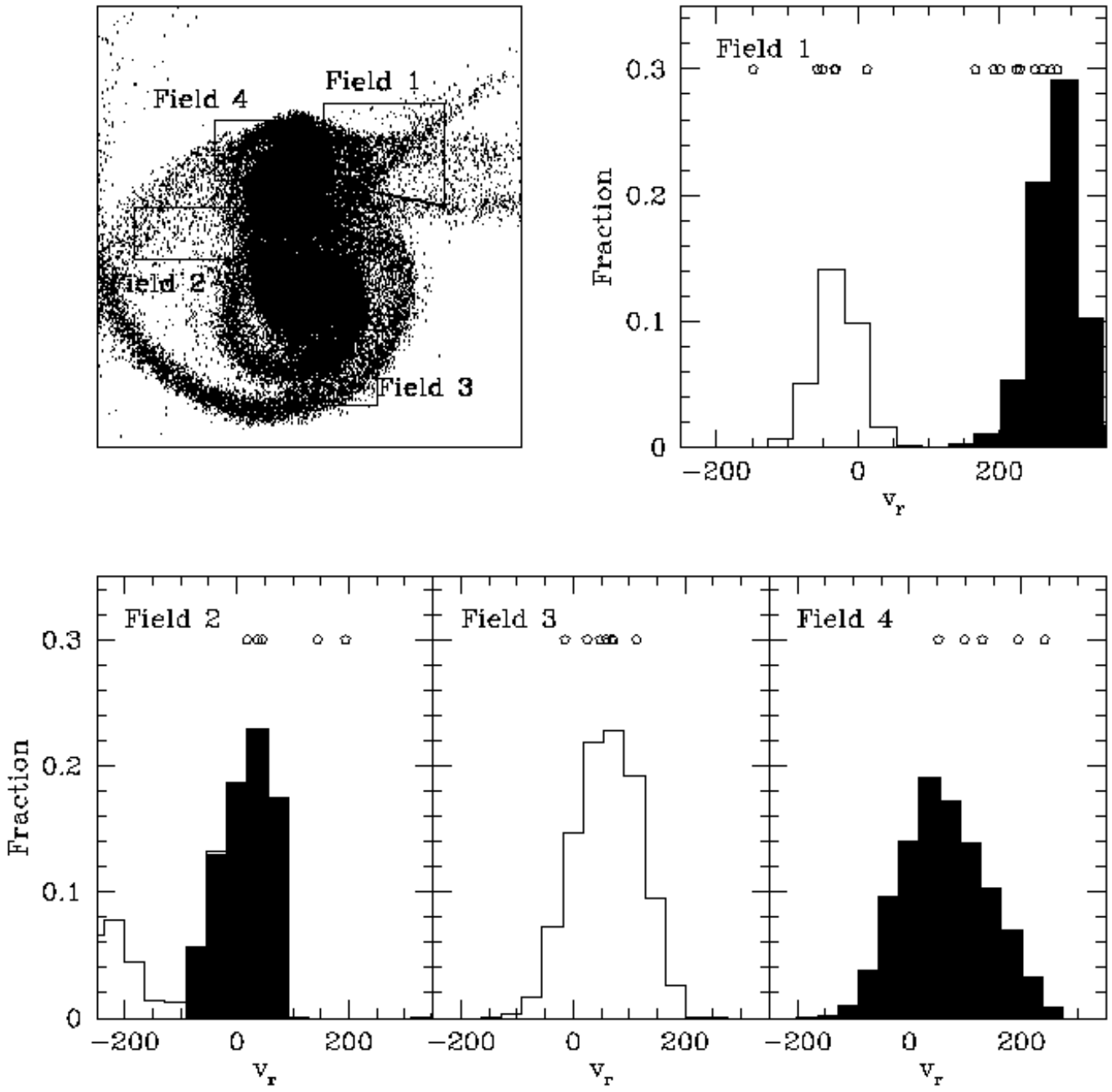

FIG. 8.— A comparison between the kinematics of our N-body model and that observed for PNe in four regions of the M51 system. The velocity scale is set by the relative velocities of NGC 5194 and 5195 (Schweizer 1977). The histograms denote disk N-body particles from NGC 5194 (open histogram) and NGC 5195 (filled histogram); the PNe velocities are represented by open pentagons. See the text for a detailed discussion of each region.

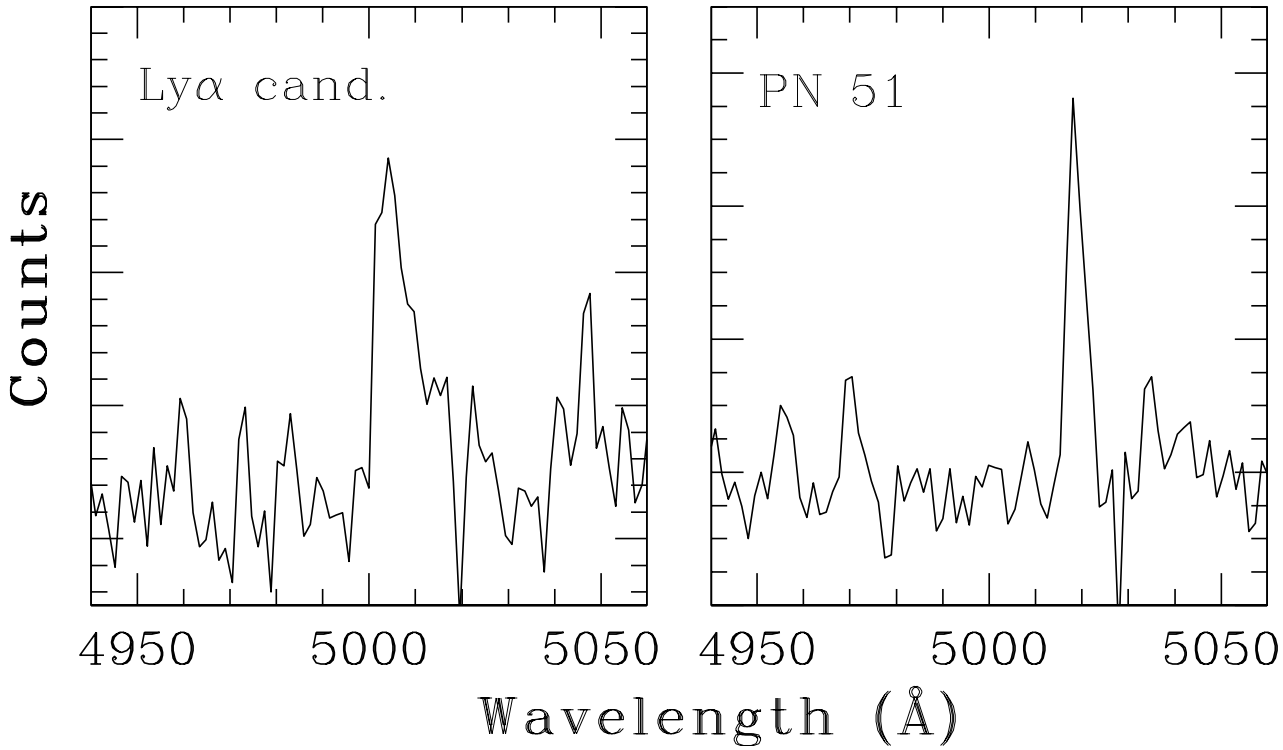

FIG. 9.— On the left is our our co-added, sky-subtracted spectrum of PN candidate 52 between the wavelengths 4940 and 5060 Å; on the right is the spectrum of PN 51. Although the objects are similarly bright in [O III] λ5007, there are clear differences in their spectral properties. We identify PN 52 as a possible Lyα galaxy at $z = 3.12$.